Whole Brain Functional Connectivity Using Multi-scale Spatio-Spectral Random Effects Model

Hakmook Kang[1,*], Xue Yang[2], Frederick W. Bryan[2], Christina M. Tripp[1], and Bennett A. Landman[2]

[1] Biostatistics, Vanderbilt University, Nashville TN, 37232 USA
[2] Electrical Engineering, Vanderbilt University, Nashville TN, 37235 USA
{Hakmook.Kang,Xue.Yang,Frederick.W.Bryan,Christina.M.Tripp,
Bennett.Landman}@vanderbilt.edu

Abstract. Functional brain networks produce connected low frequency patterns of activity when the brain is at rest which can be analyzed with resting state functional MRI (rs-fMRI) by fitting general linear models for signals acquired at a pre-defined seed region and other regions of interest (ROIs). However, typical rs-fMRI analysis tends to ignore spatial correlations in rs-fMRI data, hence biases the standard errors of estimated parameters and leads to incorrect inference. Spatio-temporal or spatio-spectral models can incorporate the spatial correlations in fMRI data. To date, these models have not targeted rs-fMRI connectivity analysis. Herein, we expand a spatio-spectral model from fMRI analysis based on several ROIs to whole brain rs-fMRI connectivity analysis. Our model captures distance-dependent local correlation (within an ROI), distance-independent global correlation (between ROIs), and temporal correlations for whole brain rs-fMRI connectivity analysis with or without confounders. Simulated and empirical experiments demonstrate that this spatio-spectral model yields valid inference for whole brain rs-fMRI connectivity analysis.

Keywords: fMRI connectivity analysis, seed analysis, spatial correlations, spectral analysis.

1 Introduction

Neuroscience and patient care have been transformed by quantitative inference of spatial-temporal brain correlations in normal and patient populations with millimeter resolution and second precision using functional MRI (fMRI) [1]. Classical statistical approaches allow mapping of brain regions associated with planning/execution, response, and default mode behaviors through task, event, and resting state paradigms, respectively [2]. When the brain is at rest (i.e., not task driven), functional networks produce correlated low frequency patterns of activity that can be observed with resting state fMRI (rs-fMRI). These correlations define one measure of functional connectivity which may be estimated by regression of activity in a region of interest (ROI) against that of the remainder of the brain [3].

Absolute voxel-wise MRI intensities (arbitrary values) are rarely used in isolation for inference – rather, the temporal and spatial patterns/correlations of changes over time are of primary interest. Statistical analyses enable *inference* of the probability

that observed signals are not observed by chance (i.e., that there exist *significant* associations between the observed signals and model of brain activity). The techniques in wide-spread use (e.g., Gaussian noise models, auto-regressive temporal correlation) ignore spatial correlations in estimating model parameters [4]. Ignoring intrinsic spatial correlation will distort the variance of estimated parameters, leading to Type I errors in the presence of positive spatial correlation or Type II errors in the presence of negative spatial correlation [5]. Traditionally, pre-processing and post-processing steps in the statistical parametric mapping pipeline partially account for the spatial correlations. For example, data are spatially smoothed with a Gaussian kernel before estimation [6] and the correlation is taken account in the inference procedures through random field theory [7].

Recently, Kang et al. [8] proposed a spatio-spectral mixed-effects model to overcome the main barrier of incorporating spatial correlations in fMRI data analysis. This model consists of fixed and random effects that capture within-ROI and between-ROI correlations. The authors demonstrated capturing the spatial and temporal correlation through simulation and empirical experiments, but the framework was limited to consideration of up to five ROIs.

Herein, we proposed a new functional connectivity analysis method incorporating the voxel-wise general linear model and ROI connectivity results (Fig. 1). By alleviating a key estimation limitation, we can expand the Kang et al spatio-spectral mixed-effects model for an arbitrary number of ROIs to a generalized model for the whole brain rs-fMRI connectivity analysis. Briefly, (1) the whole brain is shattered into small ROIs, (2) estimation is performed on each voxel accounting for within-ROI and between-ROI correlations, and (3) statistical significance is inferred on the ROI level. We evaluate our model through simulation and empirical experiments on the whole gray matter.
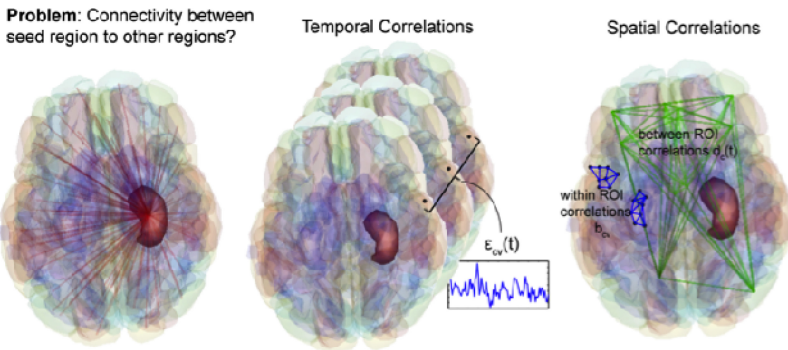
Fig. 1. The spatial and temporal model. Our goal is to discover the connectivity between a seed region and every other region in the brain. Spatial correlations model within-ROI correlations and inter-ROI correlations – these are not typically addressed in rs-fMRI. Temporal correlations are voxel-wise correlations across time – these are typically addressed in rs-fMRI analysis.

2   Theory

2.1   Model

We consider the following general spatio-temporal mixed-effects model for rs-fMRI:

$$y_{cv}(t) = \beta_{cv}^0 + (\beta_c^s + b_{cv})x_{seed}(t) + \sum_{p=1}^{P} \beta_{cv}^p x_p(t) + d_c(t) + \epsilon_{cv}(t), \qquad (1)$$

where $y_{cv}(t)$ is the rs-fMRI intensity at voxel v in ROI c at time t, x_p can be any confounders, e.g., motion parameters, $t = 1, ..., T$, $c = 1, ..., C$, and $v = 1, ..., V_c$ in ROI c. Additionally, x_{seed} is the mean time course within the seed region, β_{cv}^0 is the constant value at voxel v in ROI c across time, β_c^s is the connectivity between the seed ROI and ROI c, β_{cv}^p $(p = 1, ..., P)$ is the coefficient associated with the *p-th* confounder at voxel v in ROI c, b_{cv} is a zero-mean voxel-specific random deviation of the seed connectivity within an ROI c and this random deviation is assumed to be independent across ROIs, $d_c(t)$ is a zero-mean ROI-specific random effect which models the remaining connectivity of all other ROIs after regression of the seed ROI connectivity, and $\epsilon_{cv}(t)$ is noise that takes into account intra-voxel temporal correlation.

Under the assumption of the stationary error series $\{\epsilon_{cv}(t)\}$, the spectrum, analogous to temporal covariance matrix in the time domain, is a diagonal matrix in the Fourier domain. Therefore, we transform the model in the time domain to the frequency domain. Let the Fourier coefficients of the series $\{x_{seed}(t)\}, \{x_p(t)\}, \{d_c(t)\}$, and $\{\epsilon_{cv}(t)\}$ be $x_{seed}(\omega), x_p(\omega), d_c(\omega)$ and $\epsilon_{cv}(\omega), (\omega = \omega_1, \omega_2, ..., \omega_T)$, respectively. Then, using matrix notation in the frequency domain,

$$y(\omega) = X(\omega)(\beta + b) + Kd(\omega) + \epsilon(\omega), \qquad (2)$$

where $y(\omega) = \left[y_{11}(\omega), ..., y_{1V_1}(\omega), y_{21}(\omega), ..., y_{CV_C}(\omega)\right]^T$ is a $V_{tot} \times 1$ response vector at a frequency ω, ($V_{tot} = \sum_{c=1}^{C} V_c$, V_c is the number of voxels in ROI c), $X(\omega) = [\mathbb{I}_{V_{tot}} \otimes x_{seed}(\omega), \mathbb{I}_{V_{tot}} \otimes x_0(\omega), \mathbb{I}_{V_{tot}} \otimes x_1(\omega), ..., \mathbb{I}_{V_{tot}} \otimes x_P(\omega)]$, $\mathbb{I}_n$ denotes an $n \times n$ identity matrix, $\beta = [\beta^s, \beta^0, \beta^1, ..., \beta^P]^T$ is a $V_{tot}(P + 2) \times 1$ vector, $\beta^s = [\beta_1^s, ..., \beta_1^s, \beta_2^s, ..., \beta_2^s, ..., \beta_C^s]^T$, $\beta^p = [\beta_{11}^p, \beta_{12}^p, ..., \beta_{1V_1}^p, \beta_{21}^p, ..., \beta_{2V_2}^p, ..., \beta_{CV_C}^p]^T$ for $p \in \{0,1, ..., P\}$, $b = [b_{11}, b_{12}, ..., b_{1V_1}, b_{21}, ..., b_{CV_C}, 0, ..., ..., ..., 0]^T$ is a $V_{tot}(P + 2) \times 1$ vector, $b_c^* = [b_{c1}, b_{c2}, ..., b_{cV_c}]^T \sim N(0, \Sigma_{bc})$, $d(\omega) = [d_1(\omega), ..., d_C(\omega)]^T$, $d_j(\omega) = d_j^R(\omega) + id_j^I(\omega)$. Note that $N(\mu, \tau)$ denotes a Gaussian distribution with mean μ and variance τ, and $d^j(\omega) \sim N\left(0, \Sigma_d^j(\omega)\right), j \in \{R, I\}$, $d^R(\omega)$ and $d^I(\omega)$ are independent where R and I denote the real and imaginary part of a complex number, respectively. $K = K_1 \oplus K_2 \oplus ... \oplus K_C$, where $\oplus$ denotes direct sum and $K_j = [1, ..., 1]^T$ is a vector of length V_j whose elements are all one, $j = 1,...,C$. $\epsilon(\omega) = [\epsilon_{11}(\omega), ..., \epsilon_{1V_1}(\omega), \epsilon_{21}(\omega), ..., \epsilon_{CV_C}(\omega)]$ and $\epsilon(\omega) = \epsilon^R(\omega) + i\epsilon^I(\omega)$. *N.b.* $[\epsilon^R(\omega), \epsilon^I(\omega)]^T \sim N\left(0, \frac{1}{2}f(\omega)\mathbb{I}_{2V_{tot}}\right)$, where $f(\omega)$ is the spectrum at frequency ω.

2.2   Estimation

We define $\boldsymbol{\gamma_{cv}} = [\gamma_{cv}^s, \beta_{cv}^0, \beta_{cv}^1, \dots, \beta_{cv}^P]^T, \gamma_{cv}^s = \beta_c^s + b_{cv}^s$. The ordinary least square (OLS) estimator of $\boldsymbol{\gamma}$ is

$$\hat{\boldsymbol{\gamma}} = \left[\sum_{k=1}^T X^T(\omega_k)X(\omega_k)\right]^{-1}\left[\sum_{k=1}^T X^T(\omega_k)\boldsymbol{y}(\boldsymbol{\omega_k})\right]. \tag{3}$$

Now we need to estimate $\boldsymbol{\beta^s}$ and $\boldsymbol{b}$. To simplify, rewrite $\boldsymbol{\beta^{s*}} = [\beta_1^s, \beta_2^s, \dots, \beta_C^s]^T, \boldsymbol{b^*} = [b_{11}, b_{12}, \dots, b_{1V_1}, b_{21}, \dots, b_{CV_C}]^T$, $\Sigma_b = \Sigma_{b1} \oplus \Sigma_{b2} \oplus \dots \oplus \Sigma_{bC}$, and $\hat{\boldsymbol{\gamma}}^s = K\boldsymbol{\beta^{s*}} + \boldsymbol{b^*}$.

   To estimate $\boldsymbol{\beta}$, we do not need to estimate the exact value of $\boldsymbol{b}$ but the covariance. The covariance of $\boldsymbol{b}$ can be estimated using spatial variogram [9]. If we use empirical variogram estimation, the estimation of Σ_b will only depend on the variance of $\hat{\boldsymbol{\gamma}}^s$ across voxels within each ROI, which can be noisy. We model the spatial dependence using an exponential variogram and estimate the parameters using restricted maximum likelihood [10].

$$\hat{\boldsymbol{\beta}}^{s*} = \left[K^T \hat{\Sigma}_b^{-1} K\right]^{-1} [K^T \hat{\Sigma}_b^{-1} \hat{\boldsymbol{\gamma}^s}]. \tag{4}$$

Estimation of $\mathbf{Cov}\big(d(\omega)\big)$ and $f(\omega)$

Define $z_{cv}(\omega) = y_{cv}(\omega) - X(\omega)\boldsymbol{\gamma_{cv}}$. $z_{cv}(\omega)$ can be expressed as $d_c(\omega) + \epsilon_{cv}(\omega)$.

$$\widehat{\mathrm{Var}}\big(d_c(\omega)\big) = \widehat{\mathrm{Var}}\left(z_{c1}(\omega), \cdots, z_{cV_c}(\omega)\right), \tag{5}$$

where given locally stationary spatial process within an ROI, we compute the variance of $\boldsymbol{z}_c(\omega)$ at each frequency, which guarantees that the estimated variance is always greater than or equals to zero.

When $c \neq c'$,

$$\widehat{\mathrm{Cov}}\big(d_c(\omega), d_{c'}(\omega)\big) = \widehat{\mathrm{Cov}}(\bar{y}_c(N(\omega)), \bar{y}_{c'}(N(\omega))), \tag{6}$$

where $\bar{y}_c(\cdot)$ denotes the average of y across all the voxels in ROI c and $N(\omega)$ denotes the frequencies around a frequency ω. The size of neighbors of a frequency ω, i.e., $N(\omega)$, can be arbitrarily chosen between 1 and $T/2$ and we choose $T/8$.

The resulting covariance matrix of $\mathbf{d}(\omega)$ is guaranteed to be semi-positive definite. The spectrum for the real part or imaginary part is

$$\hat{f}^j(\omega) = [1/V_{tot}]\sum_{c=1}^C \sum_{v=1}^{V_c}\{\widehat{\mathrm{Var}}\big(z_{cv}(\omega)\big) - \hat{\sigma}_{d_c}^2\}, \tag{7}$$

where $\hat{f}^j(\omega) = \frac{1}{2}f(\omega)$, $j \in \{R, I\}$, using either the real parts or the imaginary parts of $z_{cv}(\omega)$ and $\widehat{\mathrm{Var}}\big(d_c(\omega)\big) \equiv \hat{\sigma}_{d_c}^2$, respectively. Then, a more robust estimator of the spectrum will be $\hat{f}(\omega) = [1/2]\left(\hat{f}^R(\omega) + \hat{f}^I(\omega)\right)$.

Estimation of $\mathbf{Cov}(\widehat{\boldsymbol{\beta}})$

One of the limitations of the spatio-spectral mixed-effects model in [8] is the procedure for estimating $\mathrm{Cov}(\widehat{\boldsymbol{\beta}})$ scales quadratically with the number of ROIs. Since we are interested in the coefficients for the seed time course $\boldsymbol{\beta}^{s*}$, we can simplify the covariance equations to perform the analysis on the whole brain. From OLS estimation, $\mathrm{Cov}(\widehat{\boldsymbol{\gamma}})$ is:

$$\mathrm{Cov}(\widehat{\boldsymbol{\gamma}}) = \left[\sum_{k=1}^{T} X^T(\omega_k)X(\omega_k)\right]^{-1} \left[\sum_{k=1}^{T} X^T(\omega_k)\mathrm{Cov}(\boldsymbol{y}(\omega_k))X(\omega_k)\right]\left[\sum_{k=1}^{T} X^T(\omega_k)X(\omega_k)\right]^{-1}. \tag{8}$$

The $\mathrm{Cov}(\widehat{\boldsymbol{\gamma}})$ can be arranged so that each regressor is separated: $\mathrm{Cov}(\widehat{\boldsymbol{\gamma}}) = \begin{bmatrix} \mathrm{Cov}(\widehat{\boldsymbol{\gamma}}^s) & \mathrm{Cov}(\widehat{\boldsymbol{\gamma}}^s, \widehat{\boldsymbol{\gamma}}^{0\sim P}) \\ \mathrm{Cov}(\widehat{\boldsymbol{\gamma}}^s, \widehat{\boldsymbol{\gamma}}^{0\sim P}) & \mathrm{Cov}(\widehat{\boldsymbol{\gamma}}^{0\sim P}) \end{bmatrix}$, from which we can write the covariance of the estimated seed coefficients as

$$\mathrm{Cov}(\widehat{\boldsymbol{\beta}}^{s*}) = \left[K^T\widehat{\Sigma}_b^{-1}K\right]^{-1} K^T\widehat{\Sigma}_b^{-1}\mathrm{Cov}(\widehat{\boldsymbol{\gamma}}^s)\widehat{\Sigma}_b^{-1}K\left[K^T\widehat{\Sigma}_b^{-1}K\right]^{-1}. \tag{9}$$

Let's define terms to further simplify (9) to achieve computational efficiency:

(1.) $\boldsymbol{x}(\boldsymbol{\omega}) = [x_{seed}(\omega), x_0(\omega), x_1(\omega), \ldots, x_P(\omega)]$,

(2.) $X^* = [\boldsymbol{x}(\omega_1) \quad \boldsymbol{x}(\omega_2) \quad \cdots \quad \boldsymbol{x}(\omega_T)]^T$,

(3.) $(X^{*T}X^*)^{-1}\left(\sum_{k=1}^{T}\left(x_{seed}(\omega)^2(\boldsymbol{x}(\omega_k)^T\boldsymbol{x}(\omega_k))\right)\right)(X^{*T}X^*)^{-1} \equiv A$,

(4.) $\left((X^{*T}X^*)^{-1}\boldsymbol{x}(\omega_k)^T\boldsymbol{x}(\omega_k)(X^{*T}X^*)^{-1}\right) \equiv H(\omega_k)$,

(5.) $(X^{*T}X^*)^{-1}\sum_{k=1}^{T}(f(\omega_k)\boldsymbol{x}(\omega_k)^T\boldsymbol{x}(\omega_k))(X^{*T}X^*)^{-1} \equiv Q$,

(6.) $A = \{a_{i,j}\}$, $H(\omega_k) = \{h(\omega_k)_{i,j}\}$, $Q = \{q_{i,j}\}$.

Define an operator $sum(\mathbf{M})$ that adds up all the elements in a matrix $\mathbf{M}$. Then after simplification and using the notations (1.) – (6.) above, we arrive at

$$\mathrm{Cov}(\widehat{\boldsymbol{\beta}}^{s*}) = a_{11}\begin{bmatrix} sum\left(\widehat{\Sigma_{b1}}^{-1}\right) & 0 & 0 \\ 0 & \ddots & 0 \\ 0 & 0 & sum\left(\widehat{\Sigma_{bC}}^{-1}\right) \end{bmatrix}^{-1} + \sum_{k=1}^{T}\left(h(\omega_k)_{11}\widehat{\Sigma_d}(\omega_k)\right)$$
$$+ \hat{q}_{11}\begin{bmatrix} sum\left(\widehat{\Sigma_{b1}}^{-2}\right) & 0 & 0 \\ 0 & \ddots & 0 \\ 0 & 0 & sum\left(\widehat{\Sigma_{bC}}^{-2}\right) \end{bmatrix}. \tag{10}$$

2.3 Inference

The t-test can be performed based on the estimated coefficient parameters and the covariance. Since we considered both the multi-scale spatial correlations, i.e., distance-independent between-ROI and distance-dependent within-ROI correlations, and the temporal correlations, the standard errors of parameter estimates are less likely biased. Since there are more than one ROI, it is necessary to do correction for multiple comparisons. Two widely used multiple correction methods are random field theory (RFT) and false discovery rate (FDR). RFT requires spatial smoothing of the

data and is not appropriate here because we do not employ spatial smoothing but do model the underlying spatial dependence. Therefore, we employed the FDR method for the inference on the whole brain ROIs.

3 Methods

3.1 Simulation

We simulated rs-fMRI images from Gray Matter (GM) labels with one seed ROI and 95 other ROIs. The mean connectivity coefficient for each ROI was randomly chosen from {-0.8, 0, 0.8} and no confounder was included. The connectivity coefficient for each voxel was simulated as the mean coefficient plus a zero-mean voxel-specific random effect with standard deviation 0.1. The number of voxels and the coordinates varied from ROI to ROI but the within-ROI Euclidian distance-dependent correlation structures were the same (i.e., the variogram function was the same). The between-ROI covariance was defined by a positive definite matrix in which the mean correlation was 0.2859, and minimum and maximum were -0.3652 and 0.8821, respectively. The temporal correlation was modeled by an autoregressive model (AR(1)) with the model coefficient of 0.3. The temporal signal to noise ratio (SNR) was simulated from 10 to 100 with the step size 10. The temporal SNR was defined as the ratio between mean intensity of the images to the standard deviation of the noise across time. It is noteworthy that the SNR mentioned in this paper is the temporal SNR that is typically high in rs-fMRI experiments. For each SNR level, 100 Monte Carlo simulations were performed. We calculated the false positive rate (FPR) and false negative rate (FNR) while controlling FDR at 0.05. The accuracies of estimated ROI connectivity coefficient $\widehat{\beta^s}$, within-ROI covariance $\widehat{\Sigma_b}$, and between-ROI correlations are evaluated with root mean squared error (RMSE). See Fig. 2.
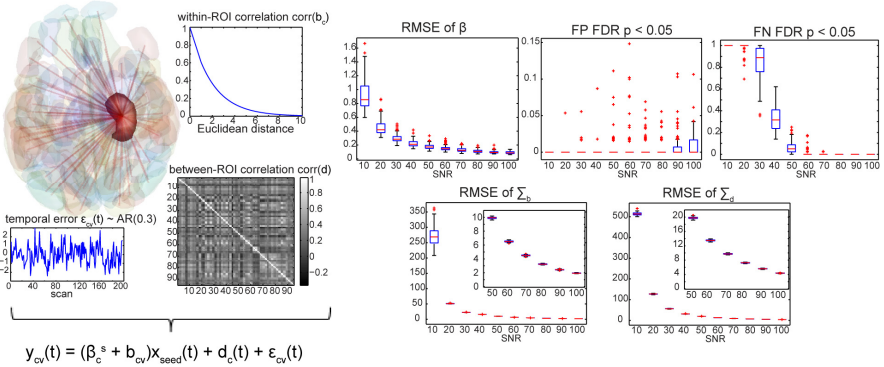
Fig. 2. Simulation setting and results. The left part displays the setting of the simulation experiment. The red region is selected as the seed region, and our interest is the connectivity between the seed region and every other 95 regions. The within-ROI correlation is plotted as a function of Euclidean distance, the between-ROI correlation is a 95 by 95 matrix, and the temporal error follows an AR(1) model with the model coefficient of 0.3. The RMSE of $\widehat{\beta^s}$, $\widehat{\Sigma_b}$ and $\widehat{\Sigma_d}$, the FP and FN with FDR correction are plotted in the right part as a function of SNR. The RMSE plots of $\widehat{\Sigma_b}$ and $\widehat{\Sigma_d}$ are enlarged for SNR from 50 to 100.

The RMSE of $\widehat{\beta^s}$ decreases exponentially as the SNR increases. The FPR of connectivity coefficients is under control for all SNR settings at FDR = 0.05. However, the FNR is 1 when SNR is very low (SNR = 10), then it decreases exponentially toward lower level as SNR increases. The RMSEs of $\widehat{\Sigma_b}$ and $\widehat{\Sigma_d}$ decrease exponentially as SNR increases.

The widely accepted seed-based method in which the time series in each ROI are averaged across voxels and functional connectivity is defined as correlation between a seed time series and the average time series in an ROI, was also applied to the simulated data at SNR = 80. Because of high SNR, the conventional method results in FNR = 0 as our method does. However, in terms of FPR, the spatio-spectral random effects model outperforms the conventional approach, i.e., FPR of 0.0327 from the conventional approach and 0.0287 from our method. This 12 percent gain in FPR confirms that ignoring the underlying positive correlation in an ROI tends to inflate false positive findings.

To further improve estimation accuracy, we considered incorporating a connectivity prior for the ROIs. In the above simulations the between-ROI correlations Σ_d could be decomposed in three components as shown in Fig. 3. We used these three components (but not their magnitudes) as a basis for $\widehat{\Sigma_d}$ in the estimation for 100 Monte Carlo simulations when SNR is 80 and compared the results with the previous results. In Fig. 3, the box plots labeled as 'no components' are our previous results and the box plots labeled as 'components' using the prior information to estimate the between ROI-correlations. As expected, the estimation of $\widehat{\Sigma_d}$ becomes more accurate while the estimation of $\widehat{\beta^s}$ and $\widehat{\Sigma_b}$ stay the same. Employing the component priors reduces FPR but increases FNR compared to 'no component'. However, the gain and loss in terms of FPR and FNR seem to be negligible. This simulation results demonstrate that utilizing additional information enhances estimation accuracy in terms of RMSE, given that the prior information of between-ROI functional connectivity is accessible and reliable.

3.2   Empirical Data Analysis

To illustrate that our spatio-spectral model can be used in empirical studies, we applied the model on a public 3T dataset with 25 healthy subjects. The rs-fMRI images acquired at 3T were downloaded from http://www.nitrc.org/projects/nyu_trt/ (197 volumes, FOV = 192 mm, flip θ = 90°, TR/TE = 2000/25 ms, 3x3x3 mm, 64x64x39 voxels) [11]. Prior to analysis, all images were corrected for slice timing artifacts and motion artifacts using SPM8 (University College London, UK). All time courses were low pass filtered at 0.1 Hz using a Chebychev Type II filter, spatially normalized to Talairach space, and linearly detrended, and de-meaned. The corresponding high resolution T1-weighted anatomical images (FOV = 256mm, flip θ = 8°, TR/TE = 2500/4.3 ms, TI = 900 ms, 176 slices) were used to acquire label images following the method described in [12,13]. The right hippocampus was selected as the seed region for each subject. The six estimated motion parameters were used as confounders. The mean estimated seed connectivity coefficient $\widehat{\beta^s}$ and the mean between-ROI correlations $\widehat{\Sigma_d}$ across 25 subjects are shown in Fig. 4. Although neither
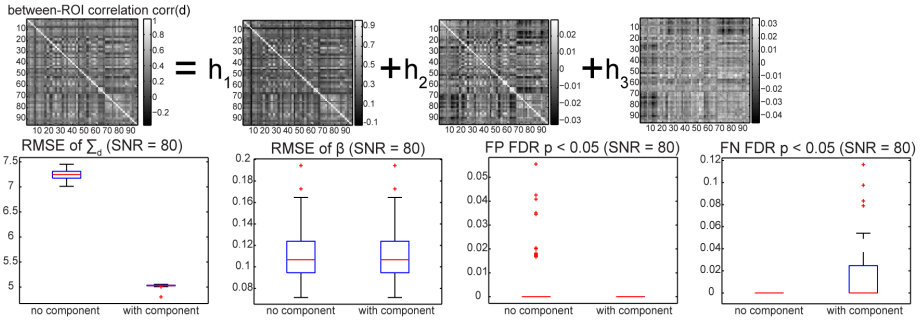
Fig. 3. Estimation with component priors. The first line shows the predefined between-ROI correlations can be decomposed by three components. The second line displays the results comparing the previous estimation without priors and the estimation with priors.

our multi-scale spatio-spectral random effects model nor the conventional approach (not presented here) can claim statistically significant functional connection to the seed region at FDR = 0.05, we demonstrate the capacity for performing the whole-brain analysis while properly considering both spatial and temporal correlations in rs-fMRI data.

4   Discussion

The proposed ROI-level analysis enables inference of brain activity associations taking into account voxel- and ROI-level dependence structure in rs-fMRI data, while typical ROI analyses narrow the problem to focus on the average time series, which ignores within- and between-ROI correlations. ROI analyses are easier to interpret since the significant regions can be mapped to and explained by the known neuroanatomy but averaging the voxel intensities reduces some voxel-wise specificity and results in incorrect inference. The proposed multi-scale spatio-spectral random effects model overlaps voxel-based and ROI-based analyses so that inference is tested on the ROI-level while the voxel-wise effects are incorporated through the random effects.
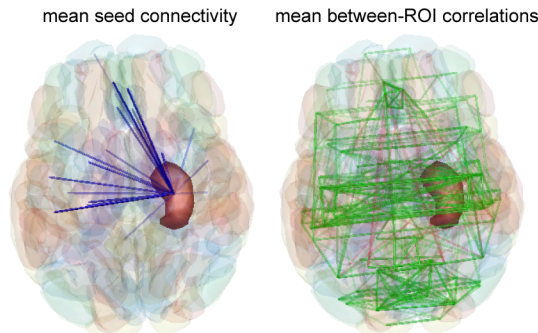
Fig. 4. Empirical Results. The red region is the seed region. The left brain shows the mean connectivity coefficient across 25 subjects. The right brain shows the mean between ROI correlations across 25 subjects.

The proposed spatio-spectral model is a sophisticated linear regression model that accounts for both spatial and temporal correlations. Spatial correlations are considered as the distance-dependent correlation structure of voxel-specific random effects within an ROI and distance-independent between-ROI correlations, i.e., multi-scale spatial correlations. The primary theoretical contributions of this work are that (1) the covariance of the estimated regression coefficients can be simplified to enable whole-brain analysis, (2) estimation of the temporal covariance can be simplified in the frequency domain, and (3) structural information on Σ_d can be used to improve estimation. Together, these contributions enable efficient and practical whole-brain spatio-spectral inference, which outperforms the widely accepted seed-based ROI analysis with averaged time series across voxels. Although the proposed framework is based on different theoretical underpinnings, the random effects general linear models of scientific interest may be used interchangeably with traditional massively univariate statistical parametric mapping (SPM).

Our model to incorporate component prior information regarding between-ROI functional dependence deserves further research in order to utilize structural information in multi-modal MRI, e.g., Diffusion Tensor Images and rs-fMRI. However, it requires caveat to use this component-based approach because non-reliable or incorrect prior information can severely distort the results, even though this can be considered as one of a few non-Bayesian approaches to directly combine functional and structural connectivity information.

References

1. Matthews, P.M., Honey, G.D., Bullmore, E.T.: Applications of fMRI in translational medicine and clinical practice. Nature Reviews Neuroscience 7, 732–744 (2006)
2. Asburner, J.T., Kibel, S.J., Nichols, T.E., Penny, W.D.: Statical parametric mapping: the analysis of functional brain images. Academic Press (2007)
3. Van Den Heuvel, M.P., Hulshoff Pol, H.E.: Exploring the brain network: a review on resting-state fMRI functional connectivity. European Neuropsychopharmacology 20, 519–534 (2010)
4. Penny, W.D., Friston, K.J., Ashburner, J.T., Kiebel, S.J., Nichols, T.E. (eds.): Statistical Parametric Mapping: The Analysis of Functional Brain Images. Academic Press, New York (2006)
5. Dubin, R.A.: Estimation of regression coefficients in the presence of spatially autocorrelated error terms. The Review of Economics and Statistics 70, 466–474 (1988)

6. Worsley, K.J., Marrett, S., Neelin, P., Vandal, A.C., Friston, K.J., Evans, A.C.: A unified statistical approach for determining significant signals in images of cerebral activation. Human Brain Mapping 4, 58–73 (1996)
7. Worsley, K.J., Evans, A.C., Marrett, S., Neelin, P.: A three-dimensional statistical analysis for CBF activation studies in human brain. Journal of Cerebral Blood Flow and Metabolism 12, 900 (1992)
8. Kang, H., Ombao, H., Linkletter, C., Long, N., Badre, D.: Spatio-spectral mixed-effects model for functional magnetic resonance imaging data. Journal of the American Statistical Association 107, 568–577 (2012)
9. Cressie, N.: Statistics for Spatial Data. Wiley (1993)
10. Lark, R., Cullis, B.: Model-based analysis using REML for inference from systematically sampled data on soil. European Journal of Soil Science 55, 799–813 (2004)
11. Shehzad, Z., Kelly, A.M.C., Reiss, P.T., Gee, D.G., Gotimer, K., Uddin, L.Q., Lee, S.H., Margulies, D.S., Roy, A.K., Biswal, B.B.: The resting brain: unconstrained yet reliable. Cerebral Cortex 19, 2209–2229 (2009)
12. Asman, A.J., Landman, B.A.: Non-local statistical label fusion for multi-atlas segmentation. Medical Image Analysis 17, 194–208 (2013)
13. Asman, A.J., Landman, B.A.: Formulating spatially varying performance in the statistical fusion framework. IEEE Transactions on Medical Imaging 31, 1326–1336 (2012)